In the paper "Earthquake hazard characterization by using entropy: application to northern Chilean earthquakes" the authors discuss a statistical physics approach for the characterization of seismicity evolution and dynamics in Northern Chile. To this end, the authors use the relationship between the Gutenberg-Richter scaling relation and the Shannon entropy to demonstrate variations in entropy associated with the occurrence of strong earthquakes in this region. The manuscript is generally well-written and organized, the methodology is sound, and the results present some interest for the scientific community. Therefore, I recommend its publication after some minor revisions listed below.

First, we would like to thank referee number 2 for his/her valuable and constructive comments.

1) In Equation 6 and so on, the upper limit of the integral, representing the interval of earthquake magnitudes, is infinity. However, there is a maximum magnitude up to which earthquakes occur. I would suggest substituting the infinity symbol with Mmax.

Thank you very much for this suggestion. Of course, it has been done.

2) In Page 4, the annotation given first to the parameter n is "the number of earthquakes with magnitude M", whereas later on "the cumulative number of earthquakes with a magnitude equal to or larger than M". The annotation given to particular parameters should be consistent throughout the text.

You have right and we have corrected this mistake to have coherence in the whole text.

3) Equation 17 has also been derived by De Santis et al. (2011). Provide the appropriate references and/or discussion.

Done. Of course, we have added De Santis et al. (2011).

4) The authors use the MAXC method to estimate the magnitude of completeness (Mc) of their catalog. Woessner and Wiemer (BSSA, 2005) suggested that Mc calculated with this method should be corrected to +0.2 units of magnitude to give more robust estimation of the b-value. Did the authors consider this correction?

Referee #2 is right in his/her appreciation: it is well known that MAXC method generally underestimated M_C value. In their paper, Woessner and Wiemer (2005) state that:" *The application of the EMR and MAXC approaches to the 1992 Landers aftershock sequence shows that Mc was slightly underestimated by 0.2 in Wiemer and Katsumata (1999)*". And, finally, their conclusions indicated: *"...for a fast analysis of Mc, we recommend using the MAXC approach in combination with the bootstrap and add a correction value (e.g., $M_C = M_C(MAXC) + 0.2$ Mc)*".

However, when the number of earthquakes to be considered is important from a statistical point of view, the best option is the MAXC technique. Thus, e.g. De Santis *et al.* (2011) stated that: "*The choice for this value of M_0 1.4 was made by inspecting the magnitude frequency and cumulative distributions* *over the period of concern to check the catalogue completeness. We recognize that this choice of M_0 is a little lower than the value given for the same region by a recent evaluation of the spatio-temporal behaviour of M_0 of the same catalogue over Italy. (...) The dense distribution of the more recent seismic network (...) and the careful check by the personnel dedicated to the operations of seismic event detection support the value here proposed for M_0. In addition, our choice of M_0 1.4 allows us to use a greater number of events than those eventually obtained considering a greater magnitude threshold, thus improving the statistics of our analysis*". (M_0 in their paper refer to M_C).

As in the case of the De Santis et al. (2011) work, the IPOC catalogue used recordings from the IPOC seismic network (GFZ & CNRS-INSU) as well as auxiliary permanent or temporary stations that were deployed in the years 2007–2014; moreover, permanent stations from the CSN (Centro Sismológico Nacional) and GEOFON (GEOFON Data Center, 1993), WestFissure network operated by the Free University of Berlin, and the MINAS and IQ networks operated by GFZ Potsdam were used. On the other hand, scientific personnel working on the IPOC network include the GFZ German Research Centre for Geosciences, Potsdam Germany; the Centre National de la Récherche Scientifíque Paris (C.N.R.S.), France; the Centro Sismológico Nacional, Chile; the Ecole Normale Supérieure, Paris, France; the Freie Universität Berlin, Germany; the GEOMAR Helmholtz Centre for Ocean Research Kiel, Germany; the Institut de Physique du Globe Paris (IPGP), France; the Pontificia Universidad Católica de Chile, Santiago, Chile; the Universidad Católica del Norte, Antofagasta, Chile and finally the Universidad de Chile, Santiago, Chile.

Although the correction of MC(MAX) + 0.2 is correct, our interest in selecting the maximum possible number of earthquakes (and their high quality), led us to slightly underestimate the value of MC.

5) As the authors discuss in Figure 9, the threshold magnitude (Mc in my previous comment) varies with depth. However, in their analysis of the entire catalog, they use a common threshold magnitude for all depth ranges. In addition, it is possible that Mc also varies with time, and it should be estimated in the temporal windows. The proper estimation of Mc (or M_0) is crucial for the determination of the b-value (see Eq. 18).

In spite of the possible depth and time variations of the GR parameters we have preferred to do just one consolidated analysis with richer statistics, representing an average behaviour of the distribution of the > 100,000 earthquakes included in this study.

6) In Figure 1 show the position of the second largest region on the globe.

Done

7) The authors mention the Gutenberg-Richter scaling relation in Fig.4, as well as in other figures (Fig.9). However, in these figures only the cumulative and discrete frequency-magnitude distribution is shown. Show also the Gutenberg-Richter relation and the associated a and b parameters.

Done

8) What do the colors indicate in Fig.6?

Usually, but it is not universal in all countries, the earthquake hazard colour code set up that “cool” colours, such as green or blue, are related with not dangerous earthquakes, whereas “hot” colour, such as orange or red, are related with earthquakes which higher magnitudes and then, the potential seismic danger is associated to them. Nevertheless, referee #2 is right and the colour could confuse the reader; therefore, we remove colour scale and now, the graph is black. For coherence, figure 3 is also redrawn in black colour.

Earthquake hazard characterization by using entropy: application to northern Chilean earthquakes

Antonio Posadas[1, 2], Denisse Pasten [3], Eugenio E. Vogel [4,5], Gonzalo Saravia[6]

[1]Departamento de Química y Física, Universidad de Almeria, 04120 Almeria, Spain.
[2]Instituto Andaluz de Geofísica, Campus Universitario de Cartuja, Universidad de Granada, 18071 Granada, Spain
[3]Departamento de Física, Facultad de Ciencias, Universidad de Chile, Santiago, Chile
[4]Departamento de Ciencias Físicas, Universidad de La Frontera, Casilla 54-D, Temuco, Chile
[5]Center for Nanoscience and Nanotechnology (CEDENNA), Santiago, Chile
[6]Los Eucaliptus 1189, Temuco 4812537, Chile

Correspondence to: Antonio Posadas (aposadas@ual.es)

Abstract. The mechanical description of the seismic cycle has an energetic analogy in terms of statistical physics and the Second Law of Thermodynamics. In this context, an earthquake can be considered as a phase transition, where continuous reorganization of stresses and forces reflects an evolution from equilibrium to non-equilibrium states and we can use this analogy to characterize the earthquake hazard of a region. In this study, we used 8 years (2007–2014) of high-quality Integrated Plate Boundary Observatory Chile (IPOC) seismic data for >100,000 earthquakes in northern Chile to test the theory that Shannon entropy, H, is an indicator of the equilibrium state of a seismically active region. We confirmed increasing H reflects the irreversible transition of a system and is linked to the occurrence of large earthquakes. Using variation in H, we could detect major earthquakes and their foreshocks and aftershocks, including 2007 M_W 7.8 Tocopilla earthquake, 2014 M_W 8.1 Iquique earthquake, and the 2010 and 2011 Calama earthquakes (M_W 6.6 and 6.8, respectively). Moreover, we identified possible periodic seismic behaviour between 80 and 160 km depth.

1 Introduction

The seismicity of a region contains abundant information that can be used, from different points of view, attempting to know when an earthquake is going to occur. In physics, Entropy is one of the most fascinating, abstract and complex concepts. The present paper shows how to use Entropy to characterize the occurrence of earthquakes, i.e. to have a characterisation of the seismic hazard in entropic terms.

It is well known (e.g. Nikulov, 2022) that the second law of thermodynamics postulates the existence of irreversible processes in physics: the total entropy of an isolated system can increase, but cannot decrease. Namely, only those phenomena for which the entropy of the universe increases are allowed. Thus, in seismology, it is natural to use entropy to find out future states that a region of the Earth's crust can access from its current state (Akopian, 2015).

The concept of entropy and its connection to the Second Law of Thermodynamics was proposed by Clausius in 1865 (Clausius, 1865) and a few years later, Boltzmann realised that entropy could be used to connect the microscopic motion of particles to the macroscopic world; in his analysis, entropy (S) is proportional to the number of accessible micro-states of the system (Ω) and is expressed by the famous Boltzmann equation:

Comentado [b1]: Correction #1 from referee #1

$$S = k \ln \Omega \ , \tag{1}$$

Comentado [b2]: Correction #2 from referee #1

where k is Boltzmann's constant. Ben-Naim (2020) stated that, at first glance, Boltzmann's entropy and Clausius' entropy are absolutely different; however, there is complete agreement in calculating changes in entropy using the two methods (up to a multiplicative constant). The generalization of Boltzmann's entropy for systems described by other macroscopic variables corresponded to Gibbs (Zupanovic and Domagoj, 2018) and can be written as:

$$S = -k \sum_{i=1}^{\Omega} p_i \log p_i \ , \tag{2}$$

where p_i is the probability of the system being in the *i-th* state. Shannon (1948) and Shannon and Weaver (1949) introduced Boltzmann-Gibbs's entropy concept into communication theory and defined the measure of information as:

$$I(p) = \sum_{i=1}^{\Omega} p_i \log p_i \ , \tag{3}$$

where p is the distribution of states and p_i is the relative frequency for each event i. The function $I(p)$ is called 'Shannon information' because it is a measure of knowledge; therefore, $-I(p)$ denotes a lack of knowledge or ignorance as Majewski (2001) has highlighted. Clearly, $I(p)$ is always negative or zero; as such, it is possible to define the 'Shannon information entropy' (H) as the negative information measure (Ben-Naim, 2017); that is:

$$H(p) = -I(p) = -\sum_{i=1}^{\Omega} p_i \, log \ p_i \ , \tag{4}$$

Comentado [b3]: Correction #3 from referee #1

which is always positive or zero. In the last equation it has been assumed, for simplicity (Truffet, 2018), that k = 1, or equivalently, that $H(p) = -\,{}^{I(p)}/_{k}$. Some (relatively) recent research carried out in the field of information theory suggests that the above expressions can be generalised. Thus, Tsallis (1988) proposed the use of:

Comentado [b4]: Correction #3 from referee #1

$$S_\tau = \frac{k}{\tau - 1}\left(1 - \sum_{i=1}^{\Omega} p_i^{\tau}\right) \ , \tag{5}$$

Comentado [b5]: Correction #3 from referee #1 where τ is called the entropic index and can, in principle, be any real number. The standard distribution that characterises Boltzmann-Gibbs statistics is a particular case of Tsallis entropy in the limit of τ = 1. Others generalizations, such as Renyi entropy, can be found in the scientific literature (e.g. Majewski and Teisseyre, 1997).

Comentado [b6]: Correction #4 form referee #1

From the point of view of classical thermodynamics (Varotsos *et al.*, 2011; Vargas *et al.*, 2015; Sarlis *et al.*, 2018; Vogel *et al.*, 2020; Telesca *et al.*, 2022, Varotsos *et al.*, 2022), but also statistical mechanics (Michas *et al.*, 2013; Vallianatos *et al.*, 2015; Papadakis *et al.*, 2015; Vallianatos *et al.*, 2016; Vallianatos *et al.*, 2018), variation in Entropy has been widely used in seismology as an indicator of the evolution of a system (from precursor papers such as Rundle *et al.*, 2003 or Sornette and Werner, 2009, to recent ones from Posadas *et al.*, 2022, Pasten *et al.*, 2022 or Posadas and Sotolongo, 2023).

In this paper, we used 8 years (2007–2014) of high-quality Integrated Plate Boundary Observatory Chile (IPOC) seismic data for >100,000 earthquakes in northern Chile to test the theory that Shannon entropy, *H*, is an indicator of the equilibrium state of a seismically active region. Moreover, we will rough out a thermodynamics vision of the seismic cycle to characterize the seismic hazard of the northern Chilean seismicity.

2 Methods

2.1 Theoretical framework

Let us start with a representation of the state of a given seismically active region from the distribution of earthquakes with magnitudes *M* associated with time *t*; that is, $P(M)$. Thus, entropy, *H*, postulated by Shannon, which is associated with information flow, can be reformulated (De Santis *et al.*, 2019) as:

$$H\,(t) = -\int_{M_0}^{M_{max}} P(M) \cdot log(P(M))dM \qquad (6)$$

Comentado [b7]: Correction #5 from referee #1 and correction #1 from referee #2

where M_0 is the threshold magnitude (i.e., the magnitude for which the seismic catalogue is complete) and M_{max} is the maximum magnitude up to which earthquakes occur. There are two restrictive conditions to solve that integral. First:

Comentado [b8]: Correction #1 from referee #2

$$\int_{M_0}^{M_{max}} P(M)dM = 1 \qquad (7)$$

Comentado [b9]: Correction #1 from referee #2

The second arises from the fact that the average value of all possible magnitudes $\bar{M}$, in a certain period, is:

$$\bar{M} = \int_{M_0}^{M_{max}} M \cdot P(M)dM \qquad (8)$$

Comentado [b10]: Correction #5 from referee #1 and correction #1 from referee #2

The Second Law of Thermodynamics requires that there exists a distribution under which H would be at its maximum value while under the two restrictive conditions; that is, the spontaneous development of the system from a state of non-equilibrium to a state of equilibrium is a process in which entropy increases and the final state of equilibrium corresponds to the maximum entropy. Thus, the problem can be solved by applying the Lagrange multiplier method; to do that, we define the lagrangian $\mathcal{L}$ as:

$$\mathcal{L}\left(P(M)\right) = H(P(M)) - \lambda_1 \int_{M_0}^{M_{max}} P(M)dM - \lambda_2 \int_{M_0}^{M_{max}} M\, P(M)\, dM \qquad (9)$$

Comentado [b11]: Correction #1 from referee #2

where λ_1 and λ_2 are Lagrange's multipliers; then, it is possible to deduce the probability density function in the form (Feng and Luo, 2009):

$$P(M) = \frac{1}{\bar{M} - M_0} \exp\left(-\frac{M - M_0}{\bar{M} - M_0}\right) \qquad (10)$$

On the other hand, if we have N earthquakes and n denotes the number of earthquakes with magnitude equal to or larger than M:

Comentado [b12]: Correction #6 from referee #1

$$P(M) = \frac{n}{N} \qquad (11)$$

then, we match both formulas and take logarithms to get:

$$\log n = \log\left(\frac{N}{\bar{M} - M_0}\right) + \frac{M_0 \cdot \log(e)}{\bar{M} - M_0} - \frac{\log(e)}{\bar{M} - M_0} \cdot M \qquad (12)$$

But, the Gutenberg-Richter relationship (Gutenberg and Richter, 1944) states that the distribution of earthquake magnitudes follows an empirical and universal relationship:

$$\log n = a - bM \qquad (13)$$

where n is the cumulative number of earthquakes with a magnitude equal to or larger than M, and a and b are real constants that may vary in space and time. Parameter a characterises the general level of seismicity in a given area during the study period (i.e., the higher the a value, the higher the seismicity), whereas parameter b, which is typically close to 1, describes the relative abundance of large to smaller shocks. Now, identifying terms from Eqs. 12 and 13, we obtain:

$$a = log\left(\frac{N}{\bar{M} - M_0}\right) + \frac{M_0 \cdot log(e)}{\bar{M} - M_0} \quad (14)$$

and

$$b = \frac{\log(e)}{\bar{M} - M_0} \quad (15)$$

Hence, the probability density function (Eq. 10) can be rewritten as:

$$P(M) = \frac{b}{\log(e)} \cdot 10^{-b(M - M_0)} \quad (16)$$

and, finally, substituting into Eq. 6, we get (De Santis *et al.*, 2011):

Comentado [b13]: Correction #3 from referee #2

$$H = -\int_{M_0}^{\infty} \frac{b \cdot 10^{-b(M - M_0)}}{\log(e)} \cdot \log\left(\frac{b \cdot 10^{-b(M - M_0)}}{log(e)}\right) dM =$$

$$= -\log(b) + \log(e \cdot log(e)) \quad (17)$$

115 After computing *b* from the classical Utsu expression (Utsu, 1965):

$$b = \frac{\log(e)}{\bar{M} - (M_0 - \frac{\Delta M}{2})} \quad (18)$$

where ΔM is the resolution of magnitude (usually $\Delta M = 0.1$), the value of entropy can be found.

2.2 Methodology

120 Our analysis approach included three steps:

1. First, the value of the threshold magnitude (M_0) is a critical choice. There are two main classes of methods to evaluate M_0: catalogue-based methods (e.g., Amorèse, 2007) and network-based methods (e.g., D'Alessandro *et al.*, 2011). We used a catalogue-based method because the necessary inputs were available from our dataset. Although some
125 studies estimate the value of M_0 by fitting the linear Gutenberg–Richter relationship to the observed frequency–magnitude distribution (the magnitude at which the lower end of the frequency–magnitude distribution departs from the Gutenberg–Richter relationship is taken as M_0 (Zúñiga and Wyss, 1995)), several other methods can better determine the threshold magnitude. Catalogue-based techniques include day-to-night noise modulation

(day/night method) (Rydele and Sacks, 1989), the Entire Magnitude Range (Ogata and Katsura, 1993), the MAXC technique or Goodness-of-Fit Test (GFT) (Wiemer and Wyss, 2000), b-value stability (MBS) (Cao and Gao, 2002), and median-based analysis of the segment slope (MBASS) (Amorèse, 2007). The MAXC technique is mainly used in applied techniques and was chosen here; however, the results do not differ significantly among these approaches.

2. Second, the time interval *W* was determined for the calculation of entropy (equation 17), using the minimum number of earthquakes to calculate *H*. The time interval can be chosen by defining a cumulative, moving, or overlapping earthquake window. Here, the results are presented for a sliding window to avoid the memory effect. It turns out that the results are substantially the same regardless of the approach taken. On the whole, the final window size offered a reasonable compromise between resolution and smoothing. The width of the window was chosen by following the approach of De Santis *et al.* (2011), which is based on meaningful values of *b*. In short, 200 events is the minimum needed to perform a robust statistical estimation of *b* and *H*. This has been confirmed by previous statistical analyses of *a* and *b* values (Utsu, 1999). However, larger values of *W* can be adopted depending on the relative error when entropy is computed (Posadas *et al.*, 2022); this criterion is explained below in the Results section.

Comentado [b14]: Correction #7 from referee # 1

3. Finally, the entropy function was obtained for each time *t* following Eq. 17. By convention, the time attributed to each point of the analyses was the time of the last seismic event considered in each window. The occurrence of a large earthquake (or the accumulation of several important ones) is expected to lead the seismic system to a state of greater disorder. Then, any earthquake is an irreversible transition to a new state carrying an increase in entropy. Once the major shock is over, entropy returns to stable values.

3 Data: the northern Chilean seismicity

The Pacific Ring of Fire, a 40,000 km horseshoe marking the tectonic boundaries of the Pacific Ocean (primarily along the boundaries of the Pacific Plate), hosts 90% of Earth's seismic activity and 75% of the active volcanoes. Also known as the Circum-Pacific Belt, it extends from Tonga and the New Hebrides islands through Indonesia, the Philippines, Japan, the Kuril and the Aleutian Islands, to the western coast of North America, before ending in the Cordillera de los Andes of South America. Among these regions, the Northern Chile Forearc experiences abundant interplate and intraplate earthquakes, intermediate and deep earthquakes associated with subduction, and a high tsunami risk along coastal areas. Events such as 2007 M_W 7.8 Tocopilla earthquake (Delouis *et al.*, 2009), 2010 M_W 8.8 Maule megathrust earthquake (Derode *et al.*, 2021), and 2014 M_W 8.1 Iquique earthquake (Cesca *et al.*, 2016) highlight the special relevance of this region. As such, monitoring seismic and volcanic activity in northern Chile using dense seismic networks (permanent and temporary) to create extensive high-quality seismic catalogues is a priority. To this end, the Integrated Plate Boundary Observatory Chile (IPOC), established by a network of European and South American institutions, operates a wide system of instruments and projects dedicated to the study of earthquakes and deformation at the continental margin of Chile (https://www.ipoc-network.org/). The network extends from the Peru–Chile border in the north to the city of Antofagasta in the south, and from the coast in the west to the high Andes in the east.

Table 1. Earthquakes with magnitudes of > 6.5 in the Integrated Plate Boundary Observatory Chile (IPOC) catalogue for the period 2007 to 2014.

Date (yyyy/mm/dd)	Time	Latitude	Longitude	Depth (km)	M_W	Name
2007/11/14	15:40:50	−22,332	−70,044	49.24	7.8	Tocopilla earthquake
2007/12/16	08:09:13	−23,298	−70,379	64.22	6.9	Aftershock of Tocopilla earthquake
2010/03/04	22:39:24	−22,391	−68,572	109.51	6.6	Calama 2010 earthquake
2011/06/20	16:35:58	−21,894	−68,554	132.84	6.8	Calama 2011 earthquake
2014/03/16	21:16:28	−19,955	−70,860	17.86	6.6	Foreshock of Iquique earthquake
2014/04/01	23:46:46	−19,589	−70,940	19.91	8.1	Iquique earthquake
2014/04/03	02:43:14	−20,595	−70,585	21.96	7.6	Aftershock of Iquique earthquake

In this study, we used high-quality IPOC data from 2007 to 2014 (the period for which data are publicly available) to test the theory that Shannon entropy (we will use Shannon entropy but whatever other such as Tsallis entropy, e.g. Vallianatos *et al.*, 2015, Vallianatos *et al.*, 2018, Khordad *et al.*, 2022 or Rastegar *et al.*, 2022 could be adopted) represents an indicator of the equilibrium state of a seismically active region (or seismic system); we hypothesized that the relationship between increasing entropy and the occurrence of large earthquakes reflects the irreversible transition of a system. The data included records of 101,601 accurately located earthquakes within an epicentral area of 17ºS–25ºS and 66ºW–72ºW (Figure 1a). A comprehensive study of the dataset can be found in Sippl *et al.* (2018).

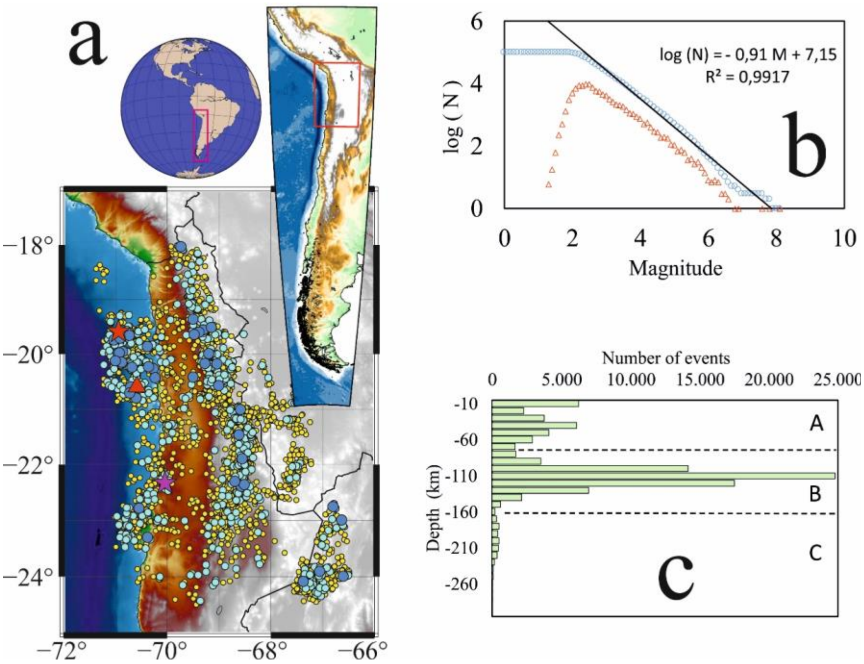

Figure 1. (a) Seismicity within an epicentral area of 17ºS–25ºS and 66ºW–72ºW between 2007 and 2014. Data are from the Integrated Plate Boundary Observatory Chile (IPOC) catalogue, which contains > 100,000 earthquakes; however, only events with magnitudes of > 4.0 are shown here (3,960 events in total). Circle colours denote event magnitudes: yellow = 4.0–4.9, cyan = 5.0–5.9, and blue = 6.0–6.9. Earthquakes with magnitudes of > 7.0 include 2007 M_W 7.8 Tocopilla earthquake (magenta star), 2014 M_W 8.1 Iquique earthquake (red star), and its main aftershock (M_W = 7.6, shown by the red triangle). (b) Gutenberg–Richter relationship. Blue circles denote the cumulative number of earthquakes; red triangles denote the non-cumulative number of earthquakes. Based on the maximum curvature (MAXC) technique (Wiemer and Wyss, 2000), $M_0 = 2.2$. (c) Histogram of earthquake depth. Bins have a 10 km resolution and three regions can be differentiated: zone A (up to 80 km depth), zone B (80–160 km depth), and zone C (> 160 km depth).

4 Results

Earthquakes included in the catalog have depths ranging from 0 to 300 km; It is evident that the seismic behavior of the shallower part is different from that of the deeper zone and so they should be analyzed separately. However, first, we begin with a preliminary analysis of the whole catalog to show whether the used technique could recognize earthquakes of greater magnitude. Subsequently, in a more detailed approach, a second analysis will be carried out that takes into account the depths (and, therefore, the different physical behaviors associated with seismicity in each region).

Comentado [UdW15]: Correction #8 and #9 from referee #1. Figure 1 include the magnitude frequency distribution (figure 4 in the original manuscript) and the depth frequency distribution (figure 8 in the original manuscript). Moreover, in figure 1c, we have added dashed lines to separate the three mentioned regions,

Correction #6 from referee #2. We show the position of the largest region on the globe. In addition, in figure 1b we show the Gutenberg-Richter relation and the associated a and b parameters.

Comentado [UdW16]: Question/issue #1 from referee #1

We added this paragraph to better explain our results, as Referee # 1 suggested.

The seismic catalogue contains 32 earthquakes with magnitudes of 6.0 or greater, 7 of which have magnitudes of > 6.5 (Table 1). The two largest earthquakes are the M_W 7.8 Tocopilla earthquake (November 14, 2007) and M_W 8.1 Iquique earthquake (April 1, 2014). Figure 2 shows a time series of events for earthquakes with magnitudes of > 4.0; the number of earthquakes versus time is shown in Figure 3.

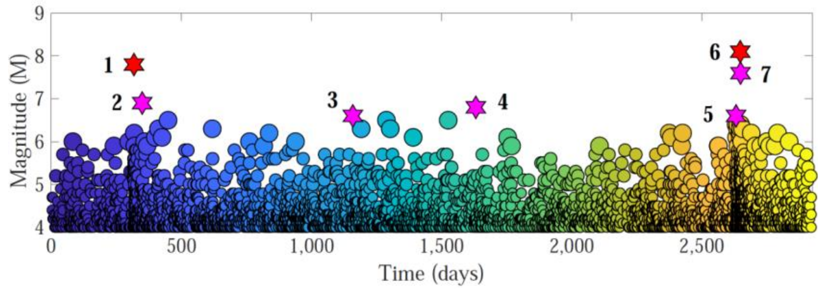

Figure 2. Magnitude versus time for earthquakes with magnitudes of > 4.0 within an epicentral area of 17ºS–25ºS and 66ºW–72ºW. Stars correspond to the earthquakes listed in Table 1, including the (1) 2007 M_W 7.8 Tocopilla earthquake, (2) 2007 M_W 6.9 Tocopilla aftershock, (3) 2010 M_W 6.6 Calama earthquake, (4) 2011 M_W 6.8 Calama earthquake, (5) M_W 6.6 foreshock of the Iquique earthquake, (6) M_W 8.1 Iquique earthquake, and (7) M_W 7.6 aftershock of the Iquique earthquake. Circles' size increases gradually with magnitude and colour, from blue to yellow, highlighting the temporal evolution.

.

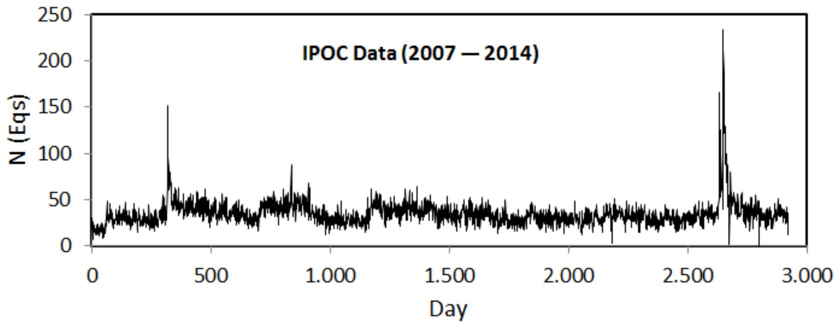

Figure 3. Number of daily earthquakes from 2007 to 2014 within an epicentral area of 17ºS–25ºS and 66ºW–72ºW. The seismic crises associated with the 2007 M_w 7.8 Tocopilla earthquake and 2014 M_w 8.1 Iquique earthquakes are clearly distinguished by the two prominent peaks.

Comentado [UdW17]: In coherence with figure 5, we remove colour scale gradient, following referee #2.

First, the threshold magnitude M_0 is needed; to get it, we used the MAXC technique as we have mentioned before. Then, the Gutenberg-Richter relationship was got (Figure 1b) and a value of $M_0 = 2.2$ is found.

The second step of our method is to determine the width of window *W* for the windowing process. Figure 4 shows the relative error of entropy versus window width. The choice of *W* must consider that values of *b* should be significant. One way to objectify this choice of *W* is to study the relative error when obtaining the entropy. Utsu's formalism (Utsu 1965) showed that the uncertainty associated with *b* value, interpreted as the error in the *b* value determination, is given by:

$$\sigma = \frac{b}{\sqrt{N}} \tag{19}$$

From the expressions 17 and 19, it is easy to get that, for an entropy value *H*, the error margins are:

$$\Delta H = \log\left(\frac{b + \Delta b}{b - \Delta b}\right) \tag{20}$$

Hence, the relative error can be calculated as:

$$\varepsilon\ (\%) = \frac{100}{H} \cdot log\left(\frac{b + \Delta b}{b - \Delta b}\right) \tag{21}$$

From Figure 4, as the window width increases, the error decreases; when the window width is 4,000 earthquakes (blue line), the error is barely 1%. Overall, the relative errors of entropy range between 0.5% and 2% for window widths of > 500 cumulative earthquakes. From this point of view, the choice of *W* must be a reasonable compromise between calculated errors and the visibility of the results. We ultimately chose a window of $W = 3{,}000$ earthquakes (yellow line), for which the relative error of entropy is close to 1% and remains practically constant.

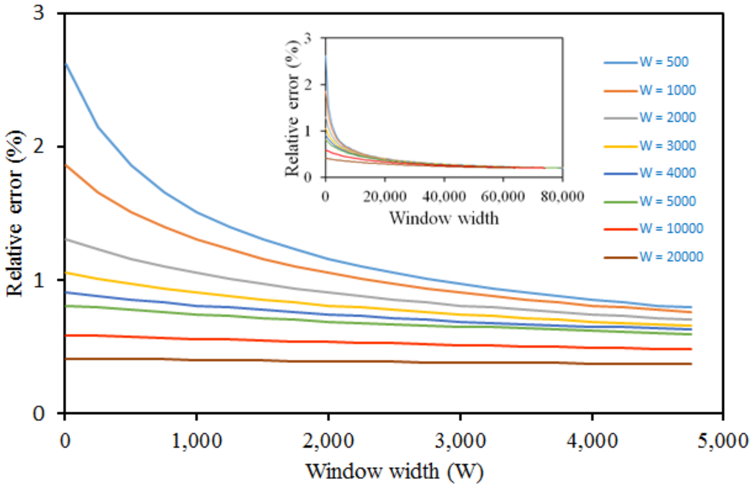

Figure 4. Relative error as a function of the given initial window width. For example, the cyan line corresponds to an initial window width of W = 500, for which the calculated relative error in entropy is 2.7%.

The threshold magnitude and width of the window for the windowing process have been set to $M_0 = 2.2$ and $W = 3{,}000$, respectively; this reduced the size of the catalogue to 84,593 events. Finally, the third step is to get Entropy H. The evolution of entropy with time from the windowing process is shown in Figure 5. Sudden changes in entropy are evident and correspond to the times of the largest earthquakes. Levels of change in the absolute values of entropy increase with increasing earthquake magnitude. The entropy change for the Tocopilla earthquake reached $H = 0.35$, while for the Calama 2010 and 2011 earthquakes, it barely exceeded $H = 0.25$. For the Iquique earthquake and its large foreshock and aftershock, the entropy value reached $H = 0.45$.

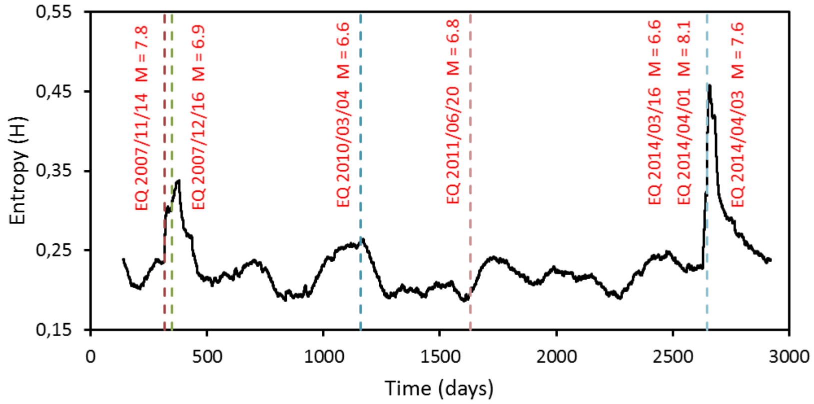

Figure 5. Time series of Shannon entropy, H, with the occurrence times of M_W > 6.5 earthquakes shown by dashed lines (note that the large foreshock, mainshock, and large aftershock of the Iquique earthquake occurred close together in time; as such, only a single dashed line is shown). Sudden changes in entropy are clearly identifiable and coincident with large earthquakes.

Comentado [UdW18]: Correction #8 from referee #3. We remove colour scale gradient.

Chilean seismicity is not only shallow seismicity; in fact, deep abundant earthquakes occur as correspond to a subduction region; then, we also investigated entropy variation as a function of earthquake type, as defined by depth (Figures 1c and 6), as follows. Zone A: intraplate earthquakes characterised by shallow depth (0–80 km) and a tectonic origin. Zone B: interplate earthquakes characterised by intermediate depth (80–160 km) and related to the contact between the two plates. Zone C: slab earthquakes that occur at large depths (> 160 km) in the slab of the underlying plate.

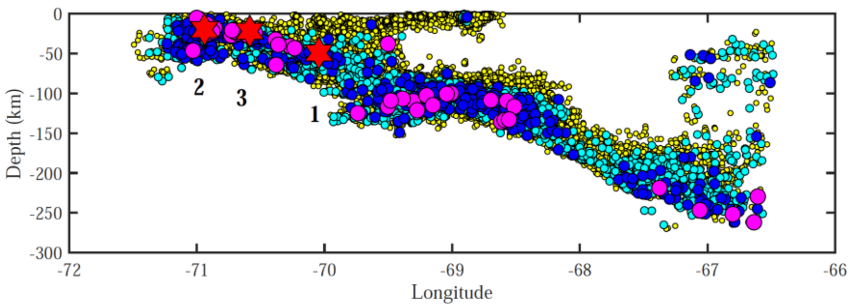

Figure 6. Earthquake depth versus longitude for earthquakes with magnitudes of > 2.0. Circle colours denote event magnitudes: yellow = 2.0–3.9, cyan = 4.0–4.9, blue = 5.0–5.9, and magenta = 6.0–6.9. Red stars denote earthquakes with magnitudes of > 7.0, including the (1) 2007 M_W 7.8 Tocopilla earthquake, (2) 2014 M_W 8.1 Iquique earthquake, and (3) 2014 M_W 7.6 aftershock of the Iquique earthquake.

The analysis of threshold magnitudes for zones A, B, and C, as well as the calculation of window *W* were as described above for the previous calculation of *H* (see Figure 7 for epicentral maps of the three zones and the computation of M_0 in each). Figure 8 shows the time series of entropy for each of the three zones. In zone A, sudden changes in entropy were coincident with the Tocopilla and Iquique earthquakes. Zones B and C show low-amplitude sawtooth fluctuations in entropy (maximum ΔH of ≤ 0.09 vs. ΔH ≈ 0.5 in zone A). The entropy variations in zones B and C are negligible compared with those in zone A.

In zone B (Figure 8), the 2010 and 2011 Calama earthquakes (M_W 6.6 and M_W 6.8 events on days 1,158 and 1,631, corresponding to April 4, 2010 and June 20, 2011, respectively) are clearly identifiable by increases in entropy. Other peaks before and after these earthquakes are coincident with either smaller earthquakes or clusters of smaller earthquakes (M_W 5.5–6.5), including a M_W 6.5 event on March 24, 2008 (day 448); a group of earthquakes between December 4, 2008 and March 27, 2009 (days 703–816, magnitudes of 5.8–6.0), a M_W 5.9 earthquake on August 8, 2012 (day 2,107); a cluster of earthquakes between July 10, 2013 and January 7, 2014 (days 2,382–2,563, magnitudes of 5.9–6.2); and, two earthquakes on March 31 and August 23, 2014, both with magnitudes of 6.2 (days 2,646 and 2,791, respectively).

A visual analysis of figure 8 seems to indicate that there is a periodic behaviour in the temporal signal of entropy; Although this behaviour seems evident in zone B, it is not so evident in zones A and C. Zone A is associated with a stress loading rate usually not uniform in time because, as is well known, the strength of the crust is not constant; Then, change in entropy is only appreciated when the two great earthquakes occurred. On the other hand, zone C, where the most complex physical phenomena occur due to the rheological state of the materials, seems to exhibit a half-period in the entropic signal, but this must be confirmed in further studies with up-to-date data. The apparent periodicity in zone B suggests carrying out a Fourier analysis of the entropic signal. The entropic signal is not uniformly sampled in the time domain; for this reason, it was averaged to the tenth part of the day and, subsequently, an interpolation was made for points with no sample. Thus, the resulting entropic signal was uniformly sampled and a fast Fourier transform was feasible.

Comentado [b19]: Question/issue #2 from referee #1

We added this paragraph to better explain our results, as Referee # 1 suggested.

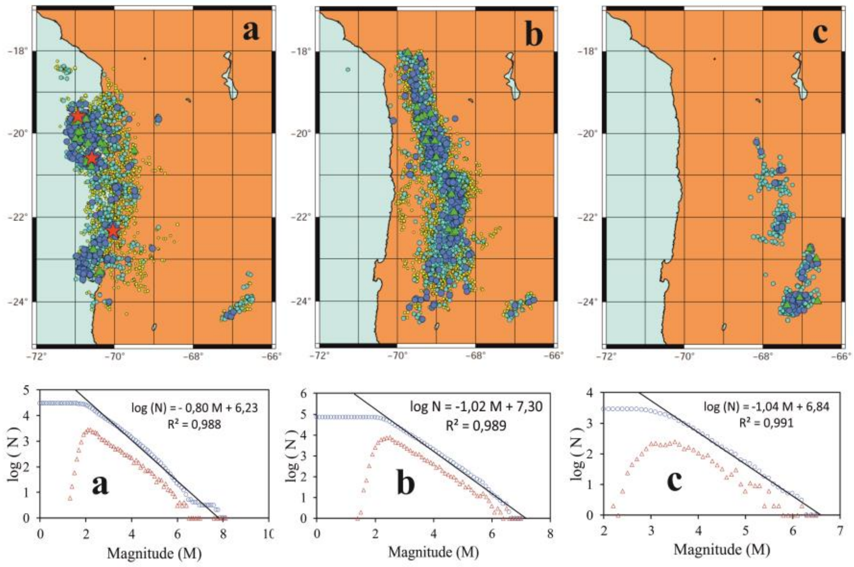

Figure 7. Epicentrally represented earthquake activity and non-cumulative and cumulative Gutenberg–Richter relationships in zones A–C for earthquakes with magnitudes of > 3.0. (a) Zone A (0–80 km), (b), zone C (80–160 km), and (c) zone C (>160 km). Symbol colours denote earthquake magnitude: yellow circles = 3.0–3.9, cyan circles = 4.0–4.9, blue circles = 5.0–5.9, green triangles = 6.0–6.9, and red stars = > 7.0. Based on the maximum curvature (MAXC) technique (Wiemer and Wyss, 2000), M_0= 2.2 in zones *A* and B, and 3.2 in zone C.

Comentado [UdW20]: Correction #7 from referee #2. Gutenberg-Richter relation and the associated a and b parameters is shown in the figure.

The Fourier transform of the entropic signal (Figure 9) revealed that the peaks of the predominant amplitude have frequencies of 0.00048 and 0.00119 $days^{-1}$, corresponding to periods of ~2,100 and 840 days, respectively. The 840-day period approximately reproduces the sequence of M > 5.5 earthquakes. For instance, 840 days after the Tocopilla earthquake (November 14, 2007) was March 3, 2010, which is 1 day before the 2010 Calama 2010. However, given the relatively short period covered by the data (8 years), this Fourier analysis is necessarily preliminary. Further studies with observation periods from 2015 until the present are needed to confirm these results.

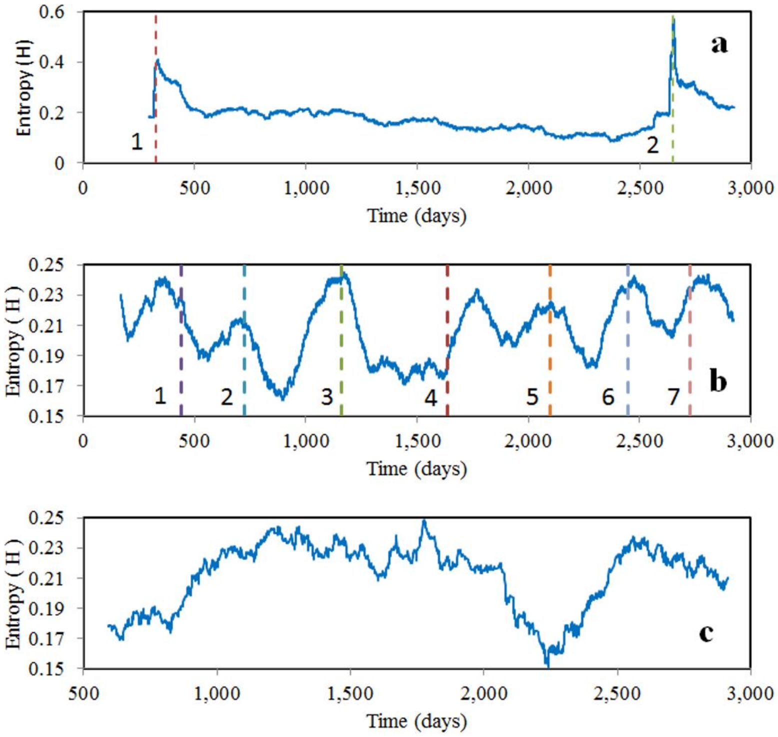

Figure 8. Time series of Shannon entropy, H, within different depth intervals. (a) Zone A (earthquakes with depths of 0–80 km), (b) zone B (80–160 km), and (c) zone C (> 160 km). The relative change in entropy in zone A is ~0.5 units compared with 0.09 units in zones B and C. Lines 1 and 2 in (a) correspond to the 2007 M_W 7.8 Tocopilla earthquake and M_W 8.1 Iquique earthquake, respectively; lines 1 to 7 in (b) correspond to the M_W 6.5 March 2008 earthquake, clusters of earthquakes with magnitudes ranging from 5.8 to 6.0 from December 2008 to March 2009, the 2010 M_W 6.6 Calama earthquake, the 2011 M_W 6.8 Calama earthquake, the 2012 M_W 5.9 earthquake, clusters of earthquakes with magnitudes ranging from 5.9 to 6.2 from July 2013 to January 201, and the two 2014 M_W 6.2 earthquakes.

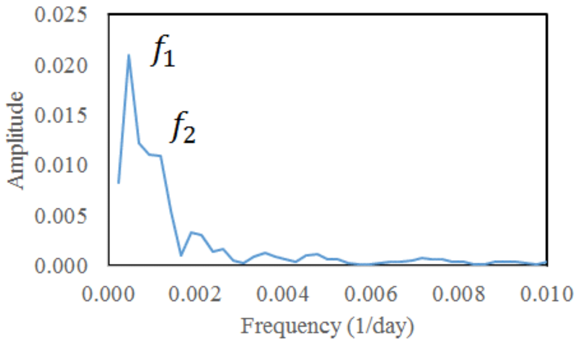

Figure 9. Spectrum for the entropic signal of zone B (80–160 km). The two peak amplitudes have frequencies of $f_1 = 0.00048\ \text{day}^{-1}$ and $f_2 = 0.00119\ \text{days}^{-1}$, corresponding to periods of ~2,100 and 840 days, respectively.

5 Discussion and conclusions

It is widely accepted that the seismic cycle (or "seismic system") comprises six main stages (Figure 10) (Derode et al., 2021; Akopian and Kocharian, 2014). The stages are: (1) Over decades or years, small and medium asperities break continuously, resulting in a uniform rate of seismicity. (2) Asperities become locked, resulting in stress accumulation and decreasing seismic activity. (3) Weeks or days before a mainshock, important asperities progressively break along some sections (i.e., the foreshock stage). (4) Over a scale of hours, accumulated stresses overcome friction and blockages in the main asperities, causing the largest magnitude earthquake of the cycle. (5) Stress relaxation occurs after the mainshock and is characterised by numerous aftershocks of smaller magnitude over several weeks or months; this ceases when new asperities become locked. (6) Finally, the system returns to the initial, long-term, state.

In this paper, we have visualized that this mechanical description of the seismic cycle has an energetic analogy in terms of statistical physics and the Second Law of Thermodynamics. As argued in detail by De Santis *et al.* (2019), an earthquake can be considered as a phase transition, where continuous reorganization of stresses and forces reflects an evolution from equilibrium to non-equilibrium states. Therefore, entropy, which measures the number of accessible states for the present conditions of the systems, can be used as an indicator of the evolution of the system (e.g., (Telesca *et al.*, 2004, Vogel *et al.*, 2020). Stages 1–3 correspond to increasing stresses and the accumulation of seismic energy. During this inter-seismic period, the magnitudes of earthquakes are relatively uniform (or 'ordered') and entropy is relatively low. When a large earthquake occurs (stage 4), the rupture process triggers earthquakes with magnitudes of all sizes in a chaotic way, evolving to new conditions reaching a wider range of microstates in a disordered way, and the entropy increases. Finally, during the post-seismic state (stages 5 and 6), the system progressively recovers conditions similar to the initial ones.

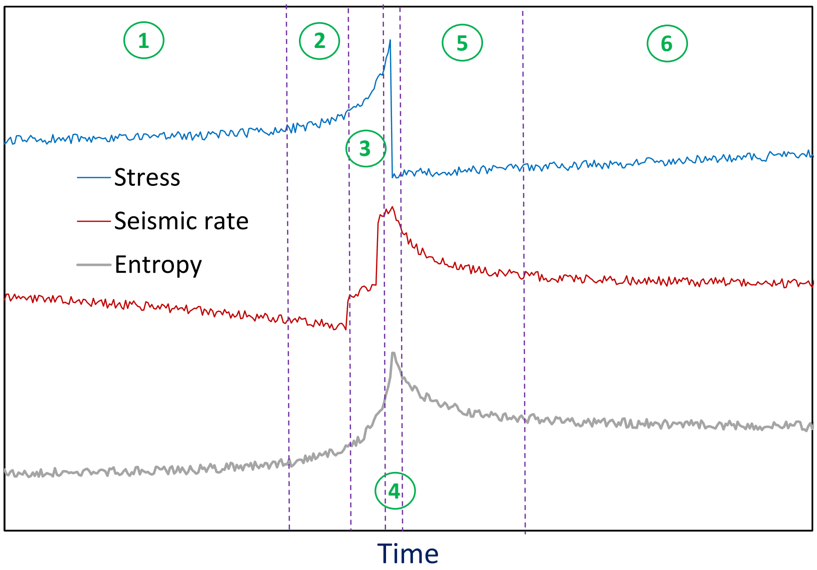

Figure 10. Seismic cycle from a mechanical perspective (i.e., stresses and seismic rate, which are shown in blue and red, respectively) and from a thermodynamic perspective (i.e., entropy, H, which is shown in grey). (1) Stage 1, the interseismic period, is characterised by approximately constant stress, seismic rate, and H. (2) Stage 2, the accumulation period, is characterised by modest increases in stress and H, but a modest decrease in seismic rate. (3) Stage 3, the foreshocks period, is characterised by increasing stress, seismic rate, and H. (4) Stage 4, the coseismic period, is characterised by an abrupt decrease in stress, but increases in the seismic rate and H. (5) Stage 5, the postseismic and aftershock period, is characterised by decreasing stress (i.e., relaxation), seismic rate, and H (towards the initial value). (6) Stage 6, during which the seismic cycle starts again.

Increasing entropy, *H*, from a thermodynamic perspective, is associated with an irreversible transition from one state to another on both small (Scholz, 1968) and large (e.g., Parsons *et al.*, 2008) scales. Using a high-quality catalogue of seismicity in northern Chile, made possible owing to the IPOC network, we confirmed a strong temporal correlation between entropy and the occurrence of earthquakes. Using the entropy value, we could identify all earthquakes with magnitudes of > 6.5 in the catalogue. (i.e., seven events from 2007 to 2014, with magnitudes ranging from 6.6 to 8.1)

However, it is important to note that changes in entropy are detected by analysing the entire catalogue; that is, to detect a change in entropy associated with any event, data from both before and after the event must be analysed. At present, this limits the use of this method for seismic prediction. Further study is needed to determine a robust approach for predicting how a time series will continue without prior knowledge; that is, to determine threshold entropy values and trends that can be used to predict a significant event in the immediate future. To achieve this, an absolute scale of entropy will be necessary.

Earthquakes in zone A (0–80 km depth) tend to be tectonic in origin and have higher magnitudes than those in zones B and C (i.e., intermediate and deep earthquakes); as such, they are of most concern from a risk management perspective. Our results show that the entropy changes associated with such events are much stronger when only data from this depth interval is considered; variations are of the order of one hundredth in zones B and C, but several tenths in zone A.

Data availability. The data are public and available at https://www.ipoc-network.org/data/ and in *Sippl et al. (2018)* available at http://doi.org/10.5880/GFZ.4.1.2018.001.

Author contributions. All authors contributed equally to the design of the methodology, discussion, analysis and revisions of the manuscript.

Competing interests. The authors declare no competing interests.

Acknowledgements. We would like to express our gratitude to the Integrated Plate Boundary Observatory Chile (IPOC) for collecting and sharing the data used in this work.

Financial support. This work was funded partially by the Spanish State Research Agency (SRA) under the grant PID2021-124701NB-C21 y C22., partially by the FEDER/UAL Project UAL2020-RNM-B1980 and also partially by the research group RNM104 of the Junta de Andalucía. The University of Almeria funding for open access charge if applicable. EEV was supported by Fondecyt (grant number 1230055) and ANID through the Center for Development of Nanoscience and Nanotechnology (CEDENNA; grant number AFB220001).

References

Akopian, S. T., Open dissipative seismic systems and ensembles of strong earthquakes: Energy balance and entropy funnels, Geophys. J. Int. 201, 1618–1641 (2015). doi.org/10.1093/gji/ggv096.

Akopian, S. Ts., Kocharian, A. N. Critical behaviour of seismic systems and dynamics in ensemble of strong earthquakes. Geophys. J. Int. 196, 580–599; doi: 10.1093/gji/ggt398 (2014).

Amorèse, D., Applying a change-point detection method on frequency-magnitude distributions, Bull. Seismol. Soc. Am. 97, 1742–1749; doi:10.1785/0120060181 (2007).

Ben-Naim, A., Entropy, Shannon's measure of information and Boltzmann's H- theorem. Entropy 2017, 19:48. doi: 10.3390/e19020048.

Ben-Naim, A., Entropy and time. Entropy 2020, 22:430. doi: 10.3390/e22040430.

Cao, A. M., Gao, S. S., Temporal variations of seismic b-values beneath northeastern japan island arc. Geophys. Res. Lett. 29(9), 1334; doi:10.1029/2001GL013775 (2002).

Cesca, S., Grigoli, F., Heimann, S., Dahm, T., Kriegerowski, M., Sobiesiak, M., Tassara, C. Olcay, M., The Mw 8.1 2014 Iquique, Chile, seismic sequence: a tale of foreshocks and aftershocks, Geophys. J. Int., 204, 1766–1780 (2016). doi: 10.1093/gji/ggv544.

Clausius, R., Mechanical theory of heat. London, UK: John van Voorst; 1865.

D'Alessandro, A., Luzio, D., D'Anna, G. & Mangano, G., Seismic Network Evaluation through Simulation: An Application to the Italian National Seismic Network, Bull. Seismol. Soc. Am. 101, 1213–1232; doi: 10.1785/0120100066 (2011).

Delouis, B., Pardo, M., Legrand, D., Monfret, T., The MW 7.7 Tocopilla Earthquake of 14 November 2007 at the Southern Edge of the Northern Chile Seismic Gap: Rupture in the Deep Part of the Coupled Plate Interface, Bull. Seismol. Soc. Am. 99, (1) 87–94; doi:10.1785/0120080192 (2009).

Derode, B., Madariaga, R., Campos, J., Seismic rate variations prior to the 2010 Maule, Chile MW 8.8 giant megathrust earthquake, Sci Rep 11, 2705. doi.org/10.1038/s41598-021-82152-0 (2021).

De Santis, A., Cianchini, G., Favali, P., Beranzoli, L. & Boschi, E., The Gutenberg-Richter Law and Entropy of Earthquakes: Two Case Studies in Central Italy, Bull. Seism. Soc. Am. 101, 1386–1395; doi: 10.1785/0120090390 (2011).

De Santis, A., Abbattista, C., Alfonsi, L., Amoruso, L., Campuzano, S., Carbone, M., Cesaroni, C., Cianchini, G., De Franceschi, G., De Santis, A., Di Giovambattista, R., Marchetti, D., Martino, L., Perrone, L., Piscini, A., Rainone, M., Soldani, M., Spogli, L., Santoro, F., "Geosystemics View of Earthquakes", Entropy 21, 412-442 (2019). doi.org/10.3390/e21040412.

Feng, L., Luo, G., The relationship between seismic frequency and magnitude as based on the Maximum Entropy Principle, Soft Comput, 2009, 13:979–83. doi: 10.10 07/s0 050 0-0 08-0340-x.

Gutenberg, B., and Richter, C. F., "Frequency of earthquakes in California", Bull. Seismol. Soc. Am., 34, 185-188, 1944.

Khordad, R., Rastegar Sedehi, H.R., Sharifzadeh, M., Susceptibility, entropy and specific heat of quantum rings in monolayer graphene: comparison between different entropy formalisms, Journal of Computational Electronics (2022) 21:422–430. doi.org/10.1007/s10825-022-01857-1.

Majewski, E., Thermodynamics of chaos and fractals applied: evolution of the earth and phase transformations. In: Teisseyre R, Majewski E, editors. Earthquake thermodynamics and phase transformations in the Earth's interior. Academic Press, 2001, p. 25–78.

Majewski, E., Teisseyre, R., Earthquake thermodynamics. Tectonophysics 1997, 277:219–33. doi: 10.1016/S0 040-1951(97)0 0 088-7.

Michas, G., Vallianatos, F., Sammonds, P., Non-extensivity and long-range correlations in the earthquake activity at the west Corinth rift (Greece). Nonlinear Process Geophys 2013, 20:713–24. dx.doi.org/10.5194/npg-20-713-2013.

Nikulov, A., The Law of Entropy Increase and the Meissner Effect. Entropy 2022, 24, 83. doi.org/10.3390/e24010083.

Ogata, Y., Katsura, K., Analysis of temporal and spatial heterogeneity of magnitude frequency distribution inferred from earthquake catalogues, Geophys. J. Int. 3(113), 727–738; doi: 10.1111/j.1365-246X.1993.tb04663.x (1993).

Papadakis, G., Vallianatos, F., Sammonds, P., A nonextensive statistical physics analysis of the 1995 Kobe, Japan earthquake. Pure Appl. Geophys 2015, 172:1923–31. dx.doi.org/10.1007/s00024-014-0876-x.

Parsons, T., Ji, C., Kirby, E., Stress changes from the 2008 Wenchuan earthquake and increased hazard in the Sichuan basin, Nature 454, 509–510; doi: 10.1038/nature07177 (2008).

Pasten, D., Saravia, G., Vogel, E., Posadas, A., Information theory and earthquakes: depth propagation seismicity in northern Chile. Chaos, Solitons and Fractals. Nonlinear Science, and Nonequilibrium and Complex Phenomena. 165, 2, 2022, 112874. doi.org/10.1016/j.chaos.2022.112874.

Posadas, A., Sotolongo-Costa, 0., Non-extensive entropy and fragment–asperity interaction model for earthquakes, Communications in Nonlinear Science and Numerical Simulation, 117, 2023, 106906. doi.org/10.1016/j.cnsns.2022.106906.

Posadas, A., Morales, J., Ibáñez, J., Posadas, A., Shaking earth: Non-linear seismic processes and the second law of thermodynamics: A case study from Canterbury (New Zealand) earthquakes, Chaos, Solitons and Fractals. Nonlinear Science, and Nonequilibrium and Complex Phenomena, 151, 2022. doi.org/10.1016/j.chaos.2021.111243.

Rastegar Sedehi, H.R., Bazrafshan, A., Khordad, R., Thermal properties of quantum rings in monolayer and bilayer graphene, Solid State Communications, 353 (2022) 114853. doi.org/10.1016/j.ssc.2022.114853.

Rundle, J.B., Turcotte, D.L., Shcherbakov, R., Klein, W., Sammis, C., Statistical physics approach to understanding the multiscale dynamics of earthquake fault systems. Rev Geophys 2003, 41:1019–49. doi:10.1029/2003RG000135.

Rydele, P. A., Sacks, I. S., Testing the completeness of earthquake catalogs and the hypothesis of self-similarity, Nature 337, 251–253; doi: 10.1038/337251a0 (1989).

Sarlis, N. V., Skordas, E. S., Varotsos, P. A., A remarkable change of the entropy of seismicity in natural time under time reversal before the super-giant M9 Tohoku earthquake on 11 March 2011, Europhys. Lett. 124, 29001–29008 (2018). doi: 10.1209/0295-5075/124/29001

Shannon, C. E., The mathematical theory of communication, Bell Syst. Tech. J. 27, 379–423 (1948).

Shannon, C. E., Weaver, W., The Mathematical Theory of Communication (The Board of Trustees of the University of Illinois, 1949).

Scholz, C. H. The frequency–magnitude relation of microfracturing in rock and its relation to earthquakes. Bull. Seismol. Soc. Am. 58, 399–415; doi: 10.1785/BSSA0580010399 (1968).

Sippl, C., Schurr, B., Asch, G., Kummerow, J., Seismicity structure of the northern Chile forearc from >100,000 double-difference relocated hypocenters, J. Geophys. Res. Solid Earth 123, 4063–4087; doi: 10.1002/2017JB015384 (2018).

Sornette D , Werner MJ . Statistical physics approaches to seismicity. In: Mey- ers RA, editor. Encyclopedia of complexity and systems science. Springer; 2009. p. 7872–91. doi: 10.1007/978-0-387-30440-3_467.

Telesca, L., Lapenna, V. & Lovallo, M. Information entropy analysis of Umbria-Marche region (central Italy). Nat. Hazards Earth Syst. Sci. 4, 691–695; 10.5194/nhess-4-691-2004 (2004).

Telesca, L., Thai, A.T., Lovallo, M., Cao, D.T., Nguyen, L.M., Shannon Entropy Analysis of Reservoir-Triggered Seismicity at Song Tranh 2 Hydropower Plant, Vietnam. Appl. Sci. 2022, 12, 8873. doi.org/10.3390/app12178873.

L. Truffet, Shannon Entropy Reinterpreted, Reports on Mathematical Physics, 81, 3, 2018, 303-319, https://doi.org/10.1016/S0034-4877(18)30050-8.

Tsallis, C., Possible generalization of Boltzmann-Gibbs statistics, J Stat Phys 1988; 52:479. doi.org/10.1007/BF01016429 .

Utsu, T., A method for determining the value of b in a formula log N = a–bM showing the magnitude-frequency relation for earthquakes, Geophys. Bull. Hokkaido Univ. Jpn. 13, 99–103 (1965).

Utsu T., Representation and Analysis of the Earthquake Size Distribution: A Historical Review and Some New Approaches, Pure Appl. Geophys. 155, 509–535; doi: 10.1007/s000240050276 (1999).

Vallianatos, F., Michas, G., Papadakis, G., A description of seismicity based on non-extensive statistical physics: a review. In: D'Amico S, editor. Earthquakes and their impact on society. Cham: Springer Natural Hazards; 2015, p. 1–41. dx.doi.org/10.1007/978-3-319-21753-6.

Vallianatos, F., Papadakis, G., Michas, G., Generalized statistical mechanics approaches to earthquakes and tectonics, Proc R Soc Lond Ser A Math Phys Eng Sci 2016; 472:20160497. http://dx.doi.org/10.1098/rspa.2016.0497.

Vallianatos, F., Michas, G., Papadakis, G., Nonextensive statistical seismology: An overview. In: Chelidze T, Vallianatos F, Telesca L, editors. Complexity of seismic time series. Complexity of seismic time series: Measurement and application, Elsevier; 2018, p. 25–59. dx.doi.org/10.1016/B978-0-12-813138-1.00002-X.

Vargas, C.A., Flores-Márquez, E.L., Ramírez-Rojas, A., Telesca, L., Analysis of natural time domain entropy fluctuations of synthetic seismicity generated by a simple stick–slip system with asperities, Physica A: Statistical Mechanics and its Applications, 419, 2015, 23-28. doi.org/10.1016/j.physa.2014.10.037.

Varotsos, P. A., Sarlis, N. V., and Skordas, E. S., “Scale-specific order parameter fluctuations of seismicity in natural time before mainshocks,” Europhys. Lett. 96, 59002, 2011. doi 10.1209/0295-5075/96/59002

Varotsos, P.A.; Sarlis, N.V.; Skordas, E.S. Order Parameter and Entropy of Seismicity in Natural Time before Major Earthquakes: Recent Results. Geosciences 2022, 12, 225. doi.org/10.3390/geosciences12060225.

Vogel, E.E., Brevis, F.G., Pastén, D., Muñoz, V., Miranda, R.A., Chian, A., Measuring the seismic risk along the Nazca-South American subduction front: Shannon entropy and mutability. Nat. Hazards Earth Syst. Sci. 20, 2943–2960. doi.org/10.5194/nhess-20-2943-2020.

Wiemer, S, Wyss, M., Minimum magnitude of complete reporting in earthquake catalogs: examples from Alaska, the Western United States, and Japan, Bull. Seismol. Soc. Am. 90, 859–869; doi: 10.1785/0119990114 (2000).

Zúñiga, F., Wyss, M., Inadvertent changes in magnitude reported in earthquake catalogs: Their evaluation through b-value estimates, Bull. Seismol. Soc. Am. 85, 1858–1866; doi:10.1785/BSSA0850061858 (1995).

Zupanovic, P., Domagoj, K., Relation between Boltzmann and Gibbs entropy and example with multinomial distribution, J. Phys. Commun. 2018, 2:045002. doi: 10.1088/2399-6528/aab7e1.